Passive Earth Pressure in Narrow Cohesive-Frictional Backfills

Li, Chutian; Lai, Fengwen ; Shiau, Jim; Keawsawasvong, Suraparb; Huang, Hanhui

DOI
10.1061/(ASCE)GM.1943-5622.0002639

Publication date
2023

Document Version
Final published version

Published in
International Journal of Geomechanics

Citation (APA)
Li, C., Lai, F., Shiau, J., Keawsawasvong, S., & Huang, H. (2023). Passive Earth Pressure in Narrow Cohesive-Frictional Backfills. *International Journal of Geomechanics*, *23*(1), Article 04022262. https://doi.org/10.1061/(ASCE)GM.1943-5622.0002639

Passive Earth Pressure in Narrow Cohesive-Frictional Backfills

Chutian Li[1]; Fengwen Lai[2]; Jim Shiau[3]; Suraparb Keawsawasvong[4]; and Hanhui Huang[5]

Abstract: A narrow backfill zone is formed when retaining walls are built near existing stabilized structures (e.g., rock faces). In such circumstances, the classical passive earth pressure coefficient is no longer applicable, and a correction factor is required for the design. This paper aims to develop analytical solutions for estimating the passive earth pressure problem of narrow cohesive-frictional backfills behind retaining walls. The novel arched differential element method considers both effects of the horizontal shear stress in backfills and the soil arching, and it is employed to estimate the passive earth pressure distribution along with wall depth. The solutions are compared against those published experimental data, analytical approaches, and finite-element limit analysis solutions. The factors influencing the distribution of passive earth pressure are also undertaken using a series of parametric studies. To implement the derived solutions into a routine design, a modified practical design equation is presented following the standard Coulomb's solutions. This work provides a theoretical guideline for the initial design of retaining walls with narrow soils, and it should be of great interest to practitioners. **DOI: 10.1061/(ASCE)GM.1943-5622.0002639**.

Author keywords: Passive earth pressure; Retaining structure; Narrow backfill; Soil arching effect; Arched differential element method; Cohesive-frictional materials.

Introduction

Traditional Rankine's and Coulomb's earth pressure theories are extensively used for the estimation of active or passive earth pressure exerted by backfills against retaining walls. A fundamental and indispensable postulation for both theories is that a triangular thrust wedge would be developed in semi-infinite frictional backfills. However, when retaining walls are constructed near rock faces (Frydman and Keissar 1987; Fan and Fang 2010; Xie et al. 2020) or existing stable structures [piles (Ni et al. 2018; Shakeel and Ng 2018), basements (Lai et al. 2022b, c), diaphragm walls (Chen et al. 2017; Li et al. 2017; Lai et al. 2020b, 2021, 2022a), etc.], the width of retained backfills is limited (termed narrow backfills) (Fig. 1). Under this context, the full development of planar slip surface from wall toe to backfill surface is unattainable, and the use of traditional theories is constrained in practice.

Over the last few decades, there have been a few published experimental works to investigate the distribution of active earth pressure exerted onto retaining walls with narrow backfills (Frydman and Keissar 1987; Take and Valsangkar 2001; O'Neal and Hagerty 2011; Yang and Tang 2017; Rui et al. 2020). The nonlinear distribution of earth pressure was observed in the measured results, which could be mainly attributed to the soil arching effect (Handy 1985). Thereafter, numerical techniques, including the finite-element method (FEM) (Fan and Fang 2010; Maleki and Imani 2022), discrete element method (Li et al. 2017; Yang and Deng 2019), and finite-element limit analysis (FELA) (Chen et al. 2019, 2020a, 2021a, b; Lai et al. 2020a; Lin et al. 2020), were used to study the failure mechanisms (e.g., number and shape of slip surfaces) and load transfer mechanisms (e.g., soil arching effect).

For the establishment of design frameworks, some analytical studies were carried out through the slip-line method (Liu and Wang 2008; Liu et al. 2009), sliding-wedge method (Chen et al. 2019, 2020b; Lai et al. 2022b), and horizontal differential element method (HDEM) (Cai et al. 2017; Chen et al. 2017, 2021b; Lin et al. 2020). Among them, HDEM is the most popular one because it considers the effect of soil arching. However, Lai et al. (2022c) and Yang et al. (2022) pointed out that the horizontal shear stress between adjacent elements is often neglected by some researchers in the force analysis when using HDEM, unavoidably causing some errors. Accordingly, they developed the arched differential element method (ADEM) and further utilized it to estimate the active earth pressure of narrow cohesive backfills behind retaining walls under the translational (T) mode (Lai et al. 2022b) and rotation about the base (RB) mode (Lai et al. 2022c), respectively. It has been proven that the ADEM method can possess higher accuracy and provide a simpler derivation and solution process, in which only the mechanical equilibrium equations are required. Moreover, a lateral stress ratio at the wall using the average vertical stress across a given differential element instead of the real vertical stress on the wall has to be adopted in the HDEM to estimate the lateral earth pressure. This unavoidably results in some deviations from reality. This drawback has also been addressed in the ADEM, as emphasized by Lai et al. (2022c) and Yang et al. (2022).

[1]Dept. of Civil and Environmental Engineering, Hong Kong Univ. of Science and Technology, Clear Water Bay, Kowloon 999077, Hong Kong; School of Civil Engineering, Chang'an Univ., Xi'an 710061, China.
[2]Institute of Geotechnical Engineering, School of Transportation, Southeast Univ., Nanjing 211189, China; Faculty of Civil Engineering and Geosciences, Delft Univ. of Technology, Building 23, Stevinweg 1/P.O. Box 5048, 2628 CN Delft/2600 GA Delft, Netherlands (corresponding author). ORCID: https://orcid.org/0000-0002-9045-0659. Email: laifengwen@163.com; f.lai-1@tudelft.nl
[3]School of Civil Engineering and Surveying, Univ. of Southern Queensland, Toowoomba, QLD 4350, Australia.
[4]Dept. of Civil Engineering, Thammasat School of Engineering, Thammasat Univ., Pathumthani 12120, Thailand.
[5]College of Civil Engineering, Fuzhou Univ., Fuzhou 350108, China.
Note. This manuscript was submitted on February 15, 2022; approved on August 14, 2022; published online on November 4, 2022. Discussion period open until April 4, 2023; separate discussions must be submitted for individual papers. This paper is part of the ***International Journal of Geomechanics***, © ASCE, ISSN 1532-3641.

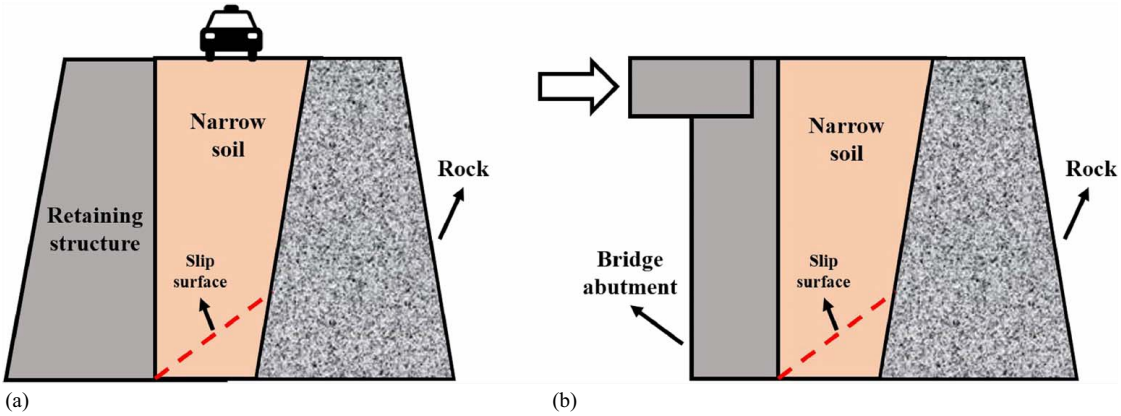

Fig. 1. Examples of the narrow backfill problem in practice: (a) highway; and (b) abutment.

Most of the previous studies focused on the active earth pressure problem in narrow frictional materials behind retaining walls. Recently, Chen et al. (2020b, 2021b) developed analytical approaches to estimate the passive earth pressure of narrow cohesionless backfills under T and RB modes both using the HDEM. It explicitly means that some deviations were still involved in their analytical framework due to the imperfections of the HDEM used, as explained previously. In addition, the contribution of soil cohesion was also neglected in their work. The research is, as a result, still going on. In all, very few works were published in relation to the passive earth pressure problem in backfill materials with limited space, in particular in cohesive backfills. Studying the passive earth pressure problem in narrow cohesive backfills is, therefore, a significant extension to present a more complete design framework of earth retaining structures from active to passive conditions.

To this end, a calculation model allowing soil arching effect and horizontal shear stress is considered in this paper for an inclined rock face (or stable retaining structures). The calculation of passive earth pressure in narrow cohesive backfills is then formulated using the ADEM. A series of parametric studies considering the effects of important design variables on the distribution of passive earth pressure are further conducted. Finally, for the practical design, we presented a fitted equation for estimating a correction factor in a more concise form to correlate with the standard Coulomb's solution.

Calculation Models and Basic Assumptions

A plane-strain calculation model is set up based on the previously reported failure mechanisms and load transfer mechanisms (Cao et al. 2019a, b; Chen et al. 2021b; Lai et al. 2022c), as shown in Fig. 2. Some basic assumptions are made for simplification, as follows:

1. A vertical rigid retaining wall is constructed around the firm and natural rock face with an inclined angle β between the rock face and the horizontal. The cohesive-frictional soils with cohesion c and friction angle ϕ are used as backfill materials. The formed trapezoid backfilling zone has a bottom width of B and a total height of H.
2. To reach a limit state of the model, the well-embedded retaining wall is assumed to be subjected to a lateral force, hence triggering the passive failure of rotating about the base (RB). For example, in practice, vibrations resulting from the construction activities and some unforeseen circumstances such as ship collisions and rock falling may occur upon bridge abutment or quay wall. RB mode may also be involved for the bridge abutment undergoing impact force from bridge deck (pavement) due to vehicle load, for diaphragm walls or sheet piles below excavation base, etc.
3. Both the wall back and the rock face are rough with various interface friction angles, defined as δ_1 and δ_2, respectively. Two factors of $\mu_1 = (\tan\delta_1/\tan\phi)$ and $\mu_2 = (\tan\delta_2/\tan\phi)$ are introduced to quantificationally characterize the interface roughness of the wall–soil interface (rotated one) and rock–soil interface (stationary one) (Lai et al. 2022c). The backfills and wall–soil interface, as well as the rock–soil interface, follow the Mohr–Coulomb (MC) failure criterion.
4. The wall is passively rotated to develop one planar failure surface with an inclined angle α_f, which can be well estimated using Coulomb's theory (Chen et al. 2021b; Lai et al. 2022c) as follows:

$$\alpha_f = \arctan\frac{1}{A + \sqrt{A(\cot\phi + A)}} \tag{1}$$

where $A = \tan(\phi + \delta_1)$.

5. The upper and lower zones are bounded by Coulomb's failure surface, with heights of H_1 and H_2, respectively. Considering the geometric relationships, height H_2 of the lower zone can be thus obtained as follows:

$$H_2 = \frac{B\tan\beta\tan\alpha_f}{\tan\beta - \tan\alpha_f} \tag{2}$$

An equation of $H_1 = H - H_2$ can be further presented.

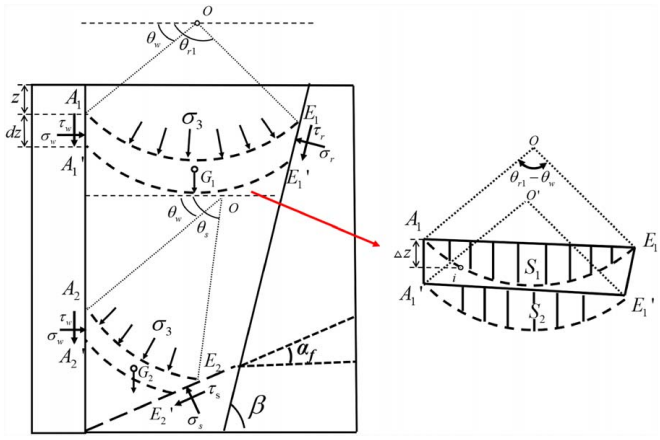

Fig. 2. Calculation model for upper and lower zones.

Therefore, this paper mainly focuses on a retaining wall with narrow backfills in which $H_2 < H$. It should be noted that, in both upper and lower zones, the rotation of the major principal stress could be postulated under the soil arching effect following a well-accepted circular-arc trajectory (Xie and Leshchinsky 2016; Lai et al. 2018; Xu et al. 2019; Cao et al. 2020).

Analytical Derivation

Stress State and Principal Stress Rotation

The stress state of backfilled soil and wall–soil/rock–soil interfaces will be changed at the limit state under the soil arching effect. It is essential to theoretically formulate the mechanism of load transfer in the retaining wall system.

For the points of A_1 and A_1', considering MC failure criterion, we have

$$\sigma_w + c\cot\phi = (\sigma_1 + c\cot\phi)\cos^2\theta_w' + (\sigma_3 + c\cot\phi)\sin^2\theta_w' \quad (3)$$

where σ_w = horizontal earth pressure; and θ_w' = rotation angle of major principle stress σ_1 in Mohr's circle (Fig. 3).

Further, according to the geometrical relations of Mohr's circle, we obtain

$$[(\sigma_w + c\cot\phi) - (\sigma_3 + c\cot\phi)]\tan\theta_w' = (\sigma_w + c\cot\phi)\tan\delta_1 \quad (4)$$

where δ_1 = friction angle of the wall–soil interface.

Combining Eqs. (3) and (4) to give

$$\tan\theta_w' = \frac{N + \tan^2\theta'_w}{N-1}\tan\delta_1 \quad (5)$$

where N = coefficient obtained by the MC failure criterion, which can be defined as follows:

$$N = \frac{\sigma_1 + c\cot\phi}{\sigma_3 + c\cot\phi} = \tan^2\left(\frac{\phi}{2} + \frac{\pi}{4}\right) \quad (6)$$

Therefore, we can solve the stress rotation angle θ_w'

$$\theta_w' = \arctan\left(\frac{N - 1 - \sqrt{(N-1)^2 - 4N\tan^2\delta_1}}{2\tan\delta_1}\right) \quad (7)$$

Similarly, the rotation angle θ_r of major principal stress of the rock–soil interface in Mohr's circle can be described as follows:

$$\theta_r = \arctan\left(\frac{N - 1 - \sqrt{(N-1)^2 - 4N\tan^2\delta_2}}{2\tan\delta_2}\right) \quad (8)$$

where δ_2 = friction angle of the rock–soil interface.

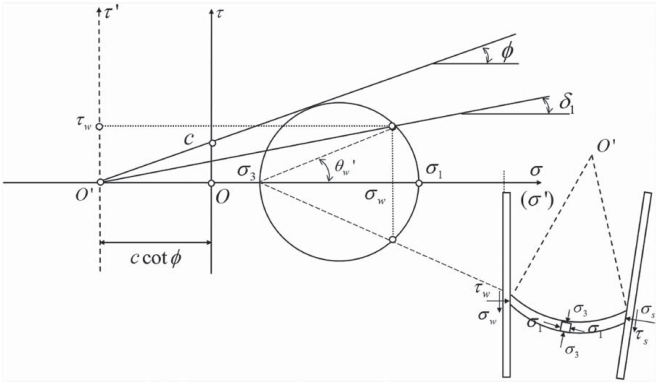

Fig. 3. Mohr circle of stress for narrow cohesive backfills.

The rotation angles θ_w and θ_{r1} of σ_1 with the horizontal for the wall–soil interface and rock–soil interface (Fig. 2) can be thus given as follows:

$$\theta_w = \frac{\pi}{2} - \theta_w' \quad (9)$$

$$\theta_{r1} = \beta + \theta_r \quad (10)$$

For Eqs. (7) and (8), we can find that both the rotation angles of σ_1 are independent of depth. That is, angles θ_w and θ_{r1} are constant along the two lateral boundaries of A_1A_1' and E_1E_1' in the upper or lower zones. Nonetheless, the rotation angle of the principal stress at any points with any depths inside the differential element would change under the effect of gravity. To characterize its effect and quantitatively formulate the soil arching effect and consider the horizontal shear stress in backfill materials, we establish an arched differential element $A_1A_1'E_1E_1'$, following a circular-arc-shaped trajectory of major principal stress rotation. The rationality of this assumption was stated in Lai et al. (2022c).

In the differential element $A_1A_1'E_1E_1'$, there is no shear stress directly acting on the upper and lower boundaries. However, compared to a horizontal element without the consideration of horizontal shear stress, the effect of shear stress has been inherently involved for an arched element following a principal stress rotation trajectory. Such simplification yields excellent convenience in the following derivation process. It can be assumed that the minor principal stress on the boundary A_1E_1 linearly increases with the height difference Δz between point A_1 and the arbitrary point i. Namely,

$$\sigma_3^i = \sigma_3^0 + \gamma\Delta z \quad (11)$$

where σ_3^0 = minor principal stress at point A_1; and σ_3^i = minor principal stress at arbitrary point i.

From Fig. 2, we can present a geometric relationship as follows:

$$\Delta z = R_{A_1E_1}(\sin\theta_w - \sin\theta) \quad (12)$$

Determination of the Geometrical Parameters

It is fundamental for the force analysis to determine the geometrical parameters involved in the arched differential element $A_1A_1'E_1E_1'$. According to the geometric relationships in Fig. 2, we have

$$\angle A_1OE_1 = \theta_{r1} - \theta_w \quad (13)$$

$$\angle OA_1A_1' = \theta_w + \frac{\pi}{2} \quad (14)$$

Combining Eqs. (13) and (14) yields

$$\angle E_1A_1A_1' = \frac{\theta_w + \theta_{r1}}{2} \quad (15)$$

Similarly, we obtain

$$\angle A_1E_1E_1' = \frac{\pi}{2} + \beta - \frac{\theta_w + \theta_{r1}}{2} \quad (16)$$

Therefore,

$$l_{A_1E_1} = \frac{H - z + B\tan\beta}{\sin\left(\frac{\theta_w + \theta_{r1}}{2}\right)} \quad (17)$$

where z = buried depth of the arched element calculated.

It should be again noted that the rotation trajectory of σ_1 is considered to be the circular arc; the radius $R_{A_1E_1}$ of the circular arc is

thus calculated using

$$R_{A_1E_1}=\frac{H-z+B\tan\beta}{2\tan\beta\sin\dfrac{\theta_w+\theta_{r1}}{2}\sin\dfrac{\theta_{r1}-\theta_w}{2}} \tag{18}$$

The height of the element $A_1A'_1E_1E'_1$ can be represented as follows:

$$h_{A_1A'_1E'_1E_1}=\sin\left(\frac{\theta_w+\theta_{r1}}{2}\right)dz \tag{19}$$

where dz = thickness of the arched element.

By observing Fig. 2, we obtain a geometrical relationship, as follows:

$$l_{E_1E'_1}=\frac{h_{A_1A'_1E'_1E_1}}{\sin\angle A_1E_1E'_1} \tag{20}$$

Substituting Eqs. (16) and (19) into Eq. (20) to get

$$l_{E_1E'_1}=\frac{\sin\left(\dfrac{\theta_w+\theta_{r1}}{2}\right)dz}{\sin\left(\dfrac{\pi}{2}+\beta-\dfrac{\theta_w+\theta_{r1}}{2}\right)} \tag{21}$$

In addition, Fig. 2 also indicates that

$$S_1=S_{\widehat{A_1E_1}}-S_{\Delta OA_1E_1}=R^2_{A_1E_1}\left[\theta_{r1}-\theta_w-\frac{\sin(\theta_{r1}-\theta_w)}{2}\right] \tag{22}$$

$$S_2=S_{\widehat{A'_1E'_1}}-S_{\Delta O'A'_1E'_1}=R^2_{A'_1E'_1}\left[\theta_{r1}-\theta_w-\frac{\sin(\theta_{r1}-\theta_w)}{2}\right] \tag{23}$$

$$S_{A_1A'_1E'_1E_1}=\frac{(l_{A_1E_1}+l_{A'_1E'_1})\sin\angle E_1A_1A'_1}{2}dz=\frac{H-z+B\tan\beta}{\tan\beta}dz \tag{24}$$

Force Analysis of the Element

The forces on the arched differential element $A_1A'_1E_1E'_1$ are derived in this section. The gravity of the element can be first calculated as follows:

$$G_1=\gamma(S_{A_1A'_1E'_1E_1}+S_2-S_1) \tag{25}$$

Substituting Eqs. (22)–(24) into Eq. (25) to yield

$$G_1=\gamma(H-z+B\tan\beta)\left\{\frac{1}{\tan\beta}-2D_1^2\left[\theta_{r1}-\theta_w-\frac{\sin(\theta_{r1}-\theta_w)}{2}\right]\right\}dz \tag{26}$$

where

$$D_1=-\frac{1}{2\tan\beta\sin\dfrac{\theta_w+\theta_{r1}}{2}\sin\dfrac{\theta_{r1}-\theta_w}{2}} \tag{27}$$

The horizontal and vertical forces acting on the lateral boundary A_1E_1 of the element are

$$F_x^{A_1E_1}=\int_{\theta_w}^{\theta_{r1}}\sigma_3^iR_{A_1E_1}\cos\theta d\theta=\sigma_3^0R_{A_1E_1}t_1+\frac{1}{2}\gamma R^2_{A_1E_1}t_1 \tag{28}$$

$$F_z^{A_1E_1}=\int_{\theta_w}^{\theta_{r1}}\sigma_3^iR_{A_1E_1}\sin\theta d\theta=\sigma_3^0R_{A_1E_1}t_2+\gamma R^2_{A_1E_1}t_3 \tag{29}$$

where

$$t_1=\sin\theta_{r1}-\sin\theta_w \tag{30}$$

$$t_2=\cos\theta_w-\cos\theta_{r1} \tag{31}$$

$$t_3=\frac{\theta_{r1}-\theta_w}{2}-\frac{\sin2\theta_{r1}+\sin2\theta_w}{4}+\cos\theta_{r1}\sin\theta_w \tag{32}$$

Similarly, we can get the horizontal and vertical forces on the boundary $A'_1E'_1$, as follows:

$$F_x^{A'_1E'_1}=\sigma_3^0Rt_1+\frac{1}{2}\gamma R^2_{A_1E_1}t_1^2+\sigma_3^0D_1t_1dz+\gamma D_1R_{A_1E_1}t_1^2dz+t_1R_{A_1E_1}d\sigma_3^0 \tag{33}$$

$$F_z^{A'_1E'_1}=\sigma_3^0R_{A_1E_1}t_2+\gamma R^2_{A_1E_1}t_3+\sigma_3^0D_1t_2dz+2\gamma D_1R_{A_1E_1}t_3dz+t_2R_{A_1E_1}d\sigma_3^0 \tag{34}$$

As emphasized previously, there is only normal stress on the upper and lower boundaries of the element. The total normal forces can be decomposed as the horizontal and vertical forces on the two boundaries:

$$F_x^{A_1A'_1}=(\sigma_w^0+c\cot\phi)dz=[(\sigma_3^0+c\cot\phi)(N\cos^2\theta'_w+\sin^2\theta'_w)-c\cot\phi]dz \tag{35}$$

$$F_z^{A_1A'_1}=(\sigma_w^0+c\cot\phi)\tan\delta_1dz=(\sigma_3^0+c\cot\phi)(N\cos^2\theta'_w+\sin^2\theta'_w)\tan\delta_1dz \tag{36}$$

$$F_x^{E_1E'_1}=-l_{E_1E'_1}\sigma_r(\tan\delta_2\cos\beta+\sin\beta)-l_{E_1E'_1}c\cos\beta \tag{37}$$

$$F_z^{E_1E'_1}=l_{E_1E'_1}(\sigma_r(\tan\delta_2\sin\beta-\cos\beta))+l_{E_1E'_1}c\sin\beta \tag{38}$$

Formulations of the Passive Earth Pressure and Thrust

Now, we have derived all the force components imposed on the element $A_1A'_1E_1E'_1$. Thereafter, two horizontal and vertical mechanical equilibrium equations can be established, as follows:

$$F_x^{A_1A'_1}-F_x^{A_1E_1}+F_x^{A'_1E'_1}+F_x^{E_1E'_1}=0 \tag{39}$$

$$F_z^{A'_1E'_1}-F_z^{A_1E_1}-F_z^{A_1A'_1}-F_z^{E_1E'_1}-G_1=0 \tag{40}$$

Substituting the nine force components written in Eqs. (26)–(28), (32), (33), and (35)–(38) into Eqs. (39) and (40) to output

$$D_2(H-z+B\tan\beta)d\sigma_3^0+D_3\sigma_3^0dz+D_4(H-z+B\tan\beta)dz+D_5dz+D_6\sigma_rdz=0 \tag{41}$$

$$D_7(H-z+B\tan\beta)d\sigma_3^0+D_8\sigma_3^0dz+D_9(H-z+B\tan\beta)dz+D_{10}dz+D_{11}\sigma_rdz=0 \tag{42}$$

where

$$D_2=-t_1D_1 \tag{43}$$

$$D_3=t_1D_1+N\cos\theta'^2_w+\sin\theta'^2_w \tag{44}$$

$$D_4=-t_1^2\gamma D_1^2 \tag{45}$$

$$D_5=c[\cot\phi(N\cos\theta'^2_w+\sin\theta'^2_w-1)-D_{12}\cos\beta] \tag{46}$$

$$D_6=-D_{12}(\sin\beta+\tan\phi\cos\beta) \tag{47}$$

$$D_7=-t_2D_1 \tag{48}$$

$$D_8=t_2D_1-(N\cos\theta'^2_w+\sin\theta'^2_w)\tan\delta_1 \tag{49}$$

$$D_9 = -\gamma\left(2t_3D_1^2 - 2D_1^2\left[\theta_{r1} - \theta_w - \frac{\sin(\theta_{r1} - \theta_w)}{2}\right] + \frac{1}{\tan\beta}\right) \quad (50)$$

$$D_{10} = -c[\cot\phi(N\cos\theta_w'^2 + \sin\theta_w'^2)\tan\delta_1 + D_{12}\sin\beta] \quad (51)$$

$$D_{11} = -D_{12}(\tan\phi\sin\beta - \cos\beta) \quad (52)$$

$$D_{12} = \frac{\sin\left(\frac{\theta_w + \theta_{r1}}{2}\right)}{\sin\left(\frac{\pi}{2} + \beta - \frac{\theta_w + \theta_{r1}}{2}\right)} \quad (53)$$

Further combining Eqs. (41) and (42) to obtain a governing equation, which can be expressed as follows:

$$D_{13}(H - z + B\tan\beta)d\sigma_3^0 + D_{14}\sigma_3^0 dz + D_{15}(H - z + B\tan\beta)dz + D_{16}dz = 0 \quad (54)$$

where

$$D_{13} = D_2D_{11} - D_7D_6 \quad (55)$$

$$D_{14} = D_3D_{11} - D_8D_6 \quad (56)$$

$$D_{15} = D_4D_{11} - D_9D_6 \quad (57)$$

$$D_{16} = D_5D_{11} - D_{10}D_6 \quad (58)$$

Eq. (54) can be rewritten as follows:

$$\frac{d\sigma_3^0}{dz} + \frac{D_{17}}{(H - z + B\tan\beta)}\sigma_3^0 + D_{18} + \frac{D_{19}}{(H - z + B\tan\beta)} = 0 \quad (59)$$

where

$$D_{17} = \frac{D_{14}}{D_{13}} \quad (60)$$

$$D_{18} = \frac{D_{15}}{D_{13}} \quad (61)$$

$$D_{19} = \frac{D_{16}}{D_{13}} \quad (62)$$

Solving Eq. (59) to give

$$\sigma_3^0 = D_{20}(H - z + B\tan\beta)^{D_{17}} + D_{21}(H - z + B\tan\beta) - D_{22} \quad (63)$$

where

$$D_{21} = \frac{D_{15}}{D_{13} - D_{14}} \quad (64)$$

$$D_{22} = \frac{D_{19}}{D_{17}} \quad (65)$$

where D_{20} = undetermined constant, which can be ensured considering σ_3^0 at $z = 0$. Therefore,

$$D_{20} = \frac{D_{22} - D_{21}(H + B\tan\beta)}{(H + B\tan\beta)^{D_{17}}} \quad (66)$$

Substituting Eq. (6) into Eq. (63) to give the lateral passive earth pressure exerted onto the wall in the upper zone, as follows:

$$\sigma_w^u = [D_{20}(H - z + B\tan\beta)^{D_{17}} + D_{21}(H - z + B\tan\beta) - D_{22} + c\cot\phi](N\cos^2\theta'_w + \sin^2\theta'_w) - c\cot\phi \quad (67)$$

The foregoing derivations have obtained the formulation of passive earth pressure in the upper zone. In reality, the force analysis for the element of $A_2A_2'E_2E_2'$ is similar to that for the element of $A_1A_1'E_1E_1'$. The main difference lies in that the lateral boundary of E_2E_2' is a Coulomb failure surface in backfills, whereas E_1E_1' is a rock–soil interface. That is, they only have various inclined angles at various buried depths due to the existence of a slip surface. To formulate the passive earth pressure in the lower zone, we need to replace $H - z + B\tan\beta$ written in all the previously related equations as $H - z$ to replace θ_{r1} as θ_s and to replace β and α_f.

It needs to be noted that θ_s is the rotation angle of σ_1 in the slip surface, which can be obtained using the geometrical relationships in Fig. 2, as follows:

$$\theta_s = \frac{\pi}{4} + \frac{\phi}{2} + \alpha_f \quad (68)$$

Repeating the aforementioned derivation process to solve the passive earth pressure in the lower zone, as described by

$$\sigma_w^l = [D'_{20}(H - z)^{D'_{15}} + D'_{21}(H - z) - D'_{22} + c\cot\phi](N\cos^2\theta'_w + \sin^2\theta'_w) - c\cot\phi \quad (69)$$

Assuming $\sigma_w^u = \sigma_w^l$ at $H = H_1$, we give

$$D'_{20} = \frac{D_{20}(H - H_1 + B\tan\beta)^{D_{17}} + D_{21}(H - H_1 + B\tan\beta) - D_{22} + D'_{22} - D'_{21}(H - H_1)}{(H - H_1)^{D'_{17}}} \quad (70)$$

where the determinations of the variables in the previous equation can be found in the Appendix.

To provide a more intuitive parameter to assess the stability against overturning of retaining structures, equations for calculating total trust of narrow soil are given as follows:

$$E_p = \int_0^{H_1}\sigma_w^u dz + \int_{H_1}^{H}\sigma_w^u dz \quad (71)$$

Eq. (71) can be normalized by the resulting geostatic stress in the dimensionless form

$$K_p = \frac{E_p}{0.5\gamma H^2} \quad (72)$$

where K_p = earth thrust coefficient, also called as earth pressure coefficient according to traditional earth pressure theories.

Implementation of Calculation Framework

The whole analytical derivation process has been shown above. To clearly show the required steps to estimate the distribution of the passive earth pressure and the passive thrust, a calculation

framework is illustrated in Fig. 4. In the flowchart, several main dimensionless design parameters (i.e., B/H, $c/\gamma H$, ϕ, μ_1, μ_2, and β) are the input variables, while σ_w^u in the upper zone and σ_w^l in the lower zone and K_p for the whole system are the output variables. To obtain the solutions, the calculation flowchart is executed by running an the calculation flowchart is executed by using a mathematical solver.

Comparison of Results

Taking a new analytical framework into practice necessitates a persuasive validation against experimental data and numerical solutions. To the best of the authors' knowledge, most of the published experimental works were focused on passive earth pressure in semi-infinite backfills. Very little can be found for narrow backfills. As a result, numerical solutions are mainly used as a benchmark for comparison and experimental data are provided for indirect comparison whenever possible.

Two numerical comparisons in purely frictional and cohesive-frictional materials are made in this section, respectively. The first comparison is shown in Fig. 5, where the relationship between the normalized earth pressure $\sigma_w/\gamma H$ and the wall depth ratio z/H is presented for purely frictional backfill materials. In this figure, the proposed solutions are compared with those of the traditional Coulomb's solution, FELA solution, FEM solution, and published experimental data and analytical solutions. The FELA and FEM models using Optum G2 (Academic Version) and Plaxis 2D (Version 2021) under the RB mode were established both based on a published model test by Ying et al. (2016) in which the model parameters were given: $c/\gamma H = 0$, $B/H = 0.8$, $\phi = 35°$, $\beta = 90°$, $\mu_1 = \mu_2 = 0.3$. The more numerical model details are omitted here and can refer to Lai et al. (2022c). The test by Ying et al. (2016) measured the passive earth pressure distribution of Fujian sand with a limited width behind the retaining wall under *T* mode. Fang et al. (1994) presented the normalized experimental results of passive earth pressure in semi-infinite soils under RB mode. It should be noted that because the scenarios of model tests chosen are somewhat different from the basic assumptions in this study, they only served as indirect comparisons. Moreover, Chen et al. (2020b) studied the passive earth pressure problem in narrow cohesionless backfills using the HDEM.

It follows from Fig. 5 that although the different modes of movement (T and RB modes) produce slight deviation with experimental data in narrow cohesionless backfills, the better agreement between the proposed solution and FELA solutions and FEM solution under RB mode is encouraging. This has greatly improved the confidence in using the current proposed solution. Interestingly, Coulomb's solution is presented based on an assumption of semi-infinite backfilling space, and it significantly underestimates the passive earth pressure exerted by narrow frictional backfills, as confirmed by the testing data in narrow backfills. This is because narrow backfills would be subjected to a stronger constraint effect than semi-infinite backfills under passive thrust. Noting that the horizontal shear force could resist the passive earth pressure in narrow backfills, but the horizontal shear force between adjacent elements was always neglected in the HDEM such that the obtained magnitude of $\sigma_w/\gamma H$ at a given depth from the HDEM is much lower than the proposed solution employing the ADEM. The comparison confirms that the proposed solution is accurate and can be used in practice with great confidence.

The second comparison is presented in Fig. 6 for narrow cohesive-frictional backfill materials. It should be noted that there is no other published experimental data that we can use to compare narrow cohesive-frictional backfill materials. To improve the confidence in the produced results of cohesive-frictional backfill materials, upper bound (UB) and lower bound (LB) FELA and FEM solutions were undertaken for comparison here. Fig. 6 shows the relationship between the normalized earth pressure $\sigma_w/\gamma H$ and the wall depth ratio z/H. Numerical comparisons in Fig. 6 show a fair to good agreement between the numerical solutions and the proposed solutions. This provides a good level of confidence in

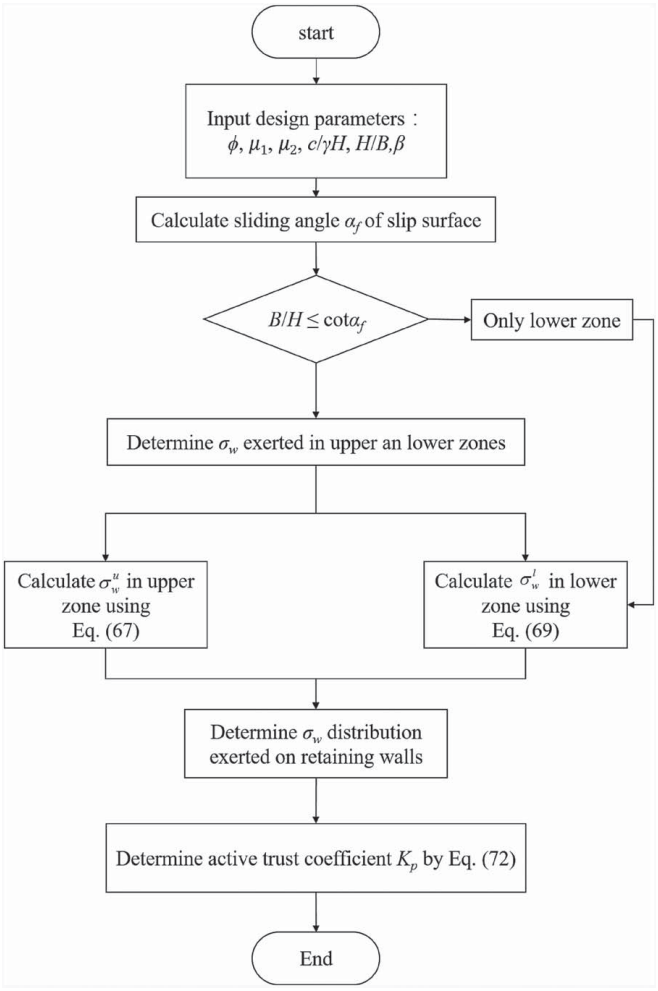

Fig. 4. Calculation flowchart.

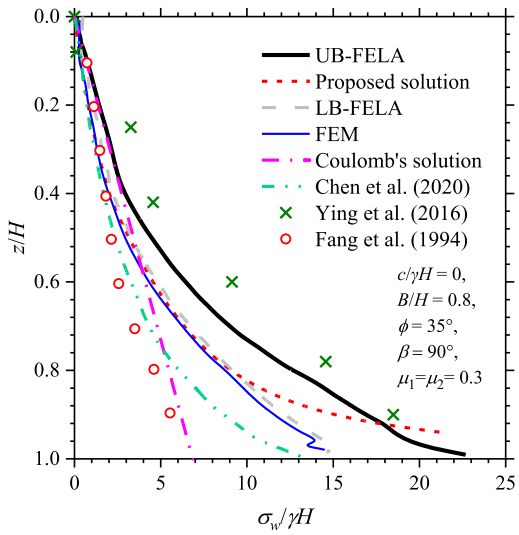

Fig. 5. Comparison of results (narrow purely frictional backfills).

the current solutions. It further strengthens the importance of considering the horizontal shear force between adjacent elements, soil arching effect, and soil cohesion in the estimation of passive earth pressure in narrow cohesive-frictional backfills.

Parametric Studies

Thoroughly understanding the factors that influence the earth pressure distribution is indispensable for the development of an accurate practical design methodology. A series of parametric studies, accounting for the effects of sensitive design parameters (e.g., aspect ratio B/H, the inclined angle of the rock face, backfills' strength parameters, and wall–soil/rock–soil interface roughness) on the distribution of passive earth pressure in narrow cohesive-frictional backfills, are thus conducted in this section. The effects of these parameters are discussed in the following sections for a base case of the aspect ratio of $B/H = 0.8$, the inclined angle of the rock face of $\beta = 60°$, the soil strength parameters ($c/\gamma H = 0.1$ and $\phi = 35°$), and the wall–soil/rock–soil interface roughness factors ($\delta_1 = \phi/3$, $\delta_2 = 2\phi/3$; hence $\mu_1 \approx 0.3$, $\mu_2 \approx 0.6$).

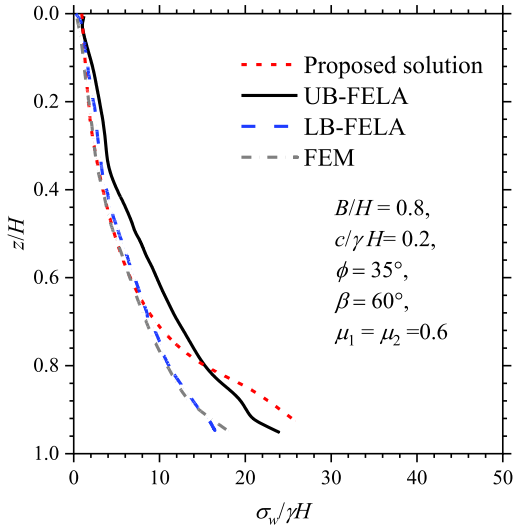

Fig. 6. Comparison of results (narrow cohesive-frictional backfills).

Effect of Aspect Ratio B/H

Fig. 7 shows the variation in normalized earth pressure $\sigma_w/\gamma H$ with wall depth z/H under various aspect ratios B/H. The difference between the narrow soils and the semi-infinite soils lies in the boundary condition of $B/H < \cot\alpha_f$. Therefore, the aspect ratio has a significant effect on the distribution of passive earth pressure. For a narrow backfill problem, the backfills are greatly constrained by the two sides of rigid walls. Such a constraint effect will be strengthened with the passive movements of retaining walls. This is also more obvious when reducing the backfill width, i.e., the retaining walls are closer to the rock faces. Theoretical results in Fig. 7 have shown that the normalized passive earth pressure $\sigma_w/\gamma H$ at a given depth increases with a decrease in B/H. It can therefore be concluded that the retaining structure with narrower backfills is subjected to greater passive resistance than that with semi-infinite ones.

Effect of Inclined Angle of the Rock Face β

Fig. 8 shows the distribution of normalized earth pressure $\sigma_w/\gamma H$ along wall depth z/H for the various inclined angle of the rock face (β). In a similar way to the H/B ratio, changing the angle β would affect the boundary condition. Although a steeper rock face results in less volume of soil to contribute to the shear stress developed for the passive earth thrust, the changes in the direction of soil movement do provide extra passive resistance in the narrow backfill problem. Accordingly, as shown in Fig. 8, the larger the β, the greater the $\sigma_w/\gamma H$. However, it should be noted that this changing law is insensitive when the inclined angle reduces to a certain degree, such as 60°, i.e., a critical angle under which the inclined angle of the rock face is less than the sliding angle α_f. In such cases, the backfill can be assumed to be semi-infinite as the full triangular thrust wedge is formed.

Effect of Backfills' Strength Parameters (c/γH and ϕ)

Figs. 9 and 10 present the variations in $\sigma_w/\gamma H$ with z/H for the various normalized soil cohesion $c/\gamma H$ and the soil friction angle ϕ,

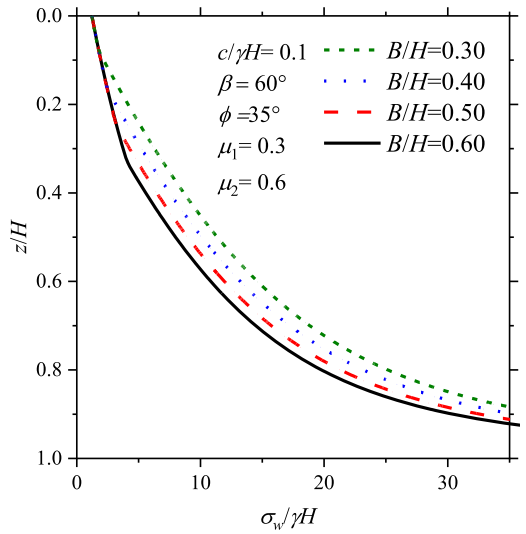

Fig. 7. Variation in normalized passive earth pressure with wall depth (various B/H values).

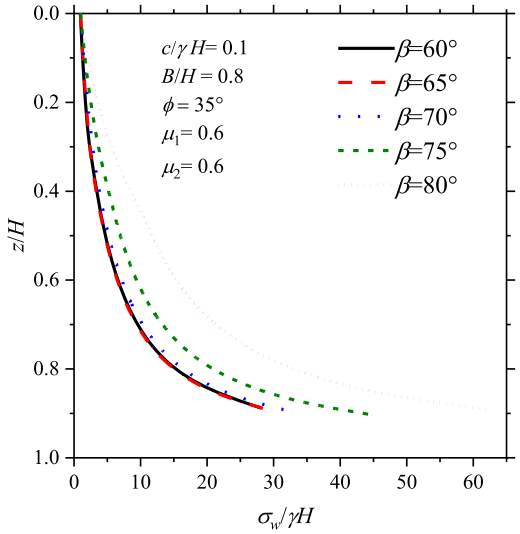

Fig. 8. Variation in normalized passive earth pressure with wall depth (various β values).

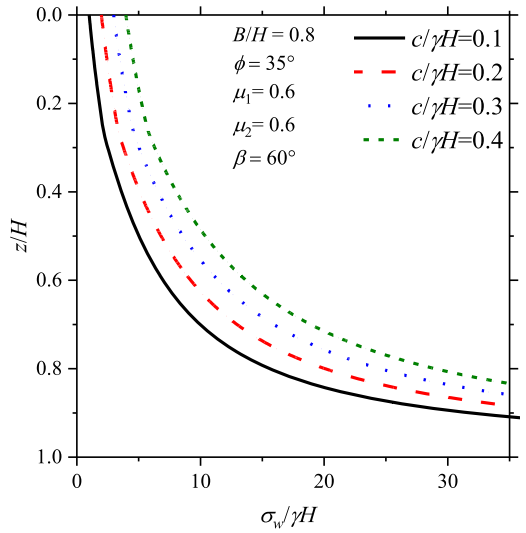

Fig. 9. Variation in normalized passive earth pressure with wall depth (various $c/\gamma H$ values).

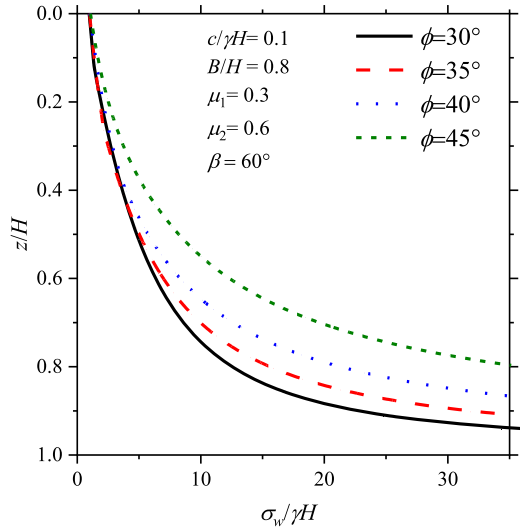

Fig. 10. Variation in normalized passive earth pressure with wall depth (various ϕ values).

respectively. Both the cohesion ratio and the friction angle represent the backfills' shear strength. The larger the soil cohesion and the soil friction angle, the greater the shear resistance. For a retaining structure subject to passive rotation, the shear stress must resist the passive earth pressure. Hence, as shown in Figs. 9 and 10, the passive earth pressure for a given depth increases with increasing $c/\gamma H$ and/or ϕ. In addition, the figures show that the rate of increase of the passive earth pressure with wall depth is greater as the soil strength parameters are larger. A possible reason for this is that an increase in soil strength parameters may enhance the soil arching effect. Therefore, greater passive earth pressure is expected to be transferred to retaining structures in light of Handy's soil arching theory (Handy 1985).

Effect of Interface Roughness Factor μ_1

The effect of the interface roughness factor on the passive earth pressure is examined in this section. The main difference between

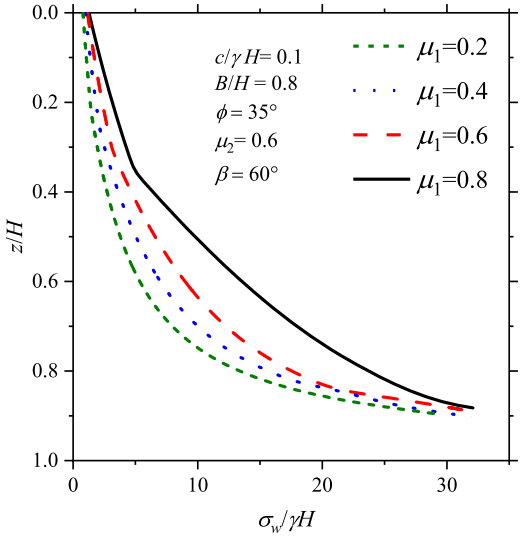

Fig. 11. Variation in normalized passive earth pressure with wall depth (various μ_1 values).

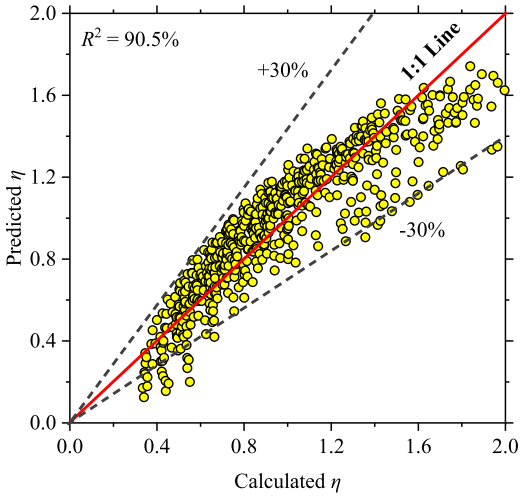

Fig. 12. Comparison of correction factor between the practical design equation and the proposed solution.

wall–soil and rock–soil interfaces is the magnitude of the roughness factors in the proposed analytical model. Consequently, we only change the roughness factor of the wall–soil interface (μ_1) in this brief study. Fig. 11 presents the distribution of the normalized passive earth pressure $\sigma_w/\gamma H$ along wall depth z/H with the varying roughness factor of the wall–soil interface (μ_1). Fig. 11 shows that a higher μ_1 yields a larger passive earth pressure at a given depth. This can be explained by the fact that the larger interface shear stress contributes to an increase in the passive earth pressure. In addition, a more stable stress arching is formed in narrow backfills as the wall–soil interface (μ_1) increases, thus mobilizing greater passive earth pressure.

Practical Design Equation

The proposed solutions subtly consider the soil arching effect and horizontal shear stress in narrow cohesive-frictional backfills behind retaining walls by using ADEM. It requires the aid of

Table 1. Optimal value of constant coefficients for closed-form approximation

p_1	p_2	p_3	p_4	p_5	p_6	p_7
3.335786	−2.66671	−4.83389	−0.94438	0.477478	0.108782	−0.78829

computer programming, which is not always available to practical geotechnical engineers. To overcome the challenge, it was suggested by Lai et al. (2022b) to present a simple design equation for practical uses. It is recommended in this paper to use the earth pressure coefficient K_p to correlate the standard Coulomb's solution $K_{p,\text{Coulomb}}$ that is widely used in practice. A correction factor η is introduced here and can be defined as follows:

$$\eta = \frac{K_p}{K_{p,\text{Coulomb}}} \tag{73}$$

To generate a data set covering a wide range of practical cases, 729 groups of calculated η in narrow cohesive-frictional backfills are calculated with the proposed solutions. The 729 groups consist of the aspect ratio ($H/B = 0.4$, 0.6, and 0.8), soil cohesion ($c/\gamma H =$ 0.00, 0.02, and 0.04), soil friction angle ($\phi = 25°$, 35°, and 45°), wall–soil interface roughness factor ($\mu_1 = 0.4$, 0.6, and 0.8), rock–soil interface roughness factor ($\mu_2 = 0.4$, 0.6, and 0.8), and inclined angle of the rock face ($\beta = 60°$, 70°, and 80°). Subsequently, a practical design equation is further developed with the aid of the method of curve fitting. The closed-form approximation can be expressed as follows:

$$\eta = p_1 + p_2 \tan^2\varphi + p_3\mu_1^2 + p_4\mu_2^2 + p_5\left(\frac{B}{H}\right)^2 + p_6\left(\frac{c}{\gamma H}\right)^2 + p_7 \tan^2\beta \tag{74}$$

where p_1–p_7 = constant coefficients. These are given in Table 1.

A comparison between the calculated η from the proposed solutions and the predicted η from the fitted Eq. (74) is shown in Fig. 12. It follows from Fig. 12 that a high coefficient of determination ($R^2 = 90.5\%$) can be found, giving greater confidence for practical uses in estimating the earth pressure at any wall depths in narrow cohesive-frictional backfills behind retaining walls using the following equation:

$$\sigma_w = \eta K_{p,\text{Coulomb}}\gamma z \tag{75}$$

Conclusions

The ADEM proposed by Lai et al. (2022b) for estimating active earth pressure in narrow c–ϕ soils has been successfully extended to formulate the distribution of passive earth pressure along the wall depth in this paper. In particular, the proposed solutions consider the effects of soil cohesion, soil arching, and horizontal shear stress, where a retaining wall was constructed near inclined rough rock faces (or other stable retaining structures). Some shortcomings of the HDEM have been well considered, and the solutions have been improved by using the ADEM. The comparisons have shown that the novel solutions are in good agreement with published experimental data, existing analytical approaches, and FELA solutions in both purely frictional and cohesive-frictional materials.

A series of parametric studies are further carried out to examine the factors influencing the magnitude and distribution of the passive earth pressure. It is found that the magnitude of passive earth pressure is governed by the constraint effect and shear resistance provided by backfills and interfaces. An interesting phenomenon is that the retaining structure with narrower backfills is subjected to greater passive resistance than that with semi-infinite ones. The study results indicate that the passive earth pressure would decrease with a reduction in the inclined angle of the rock face, wall–soil/rock–soil interface roughness factors, and soil strength parameters. An increase in the backfill width aspect ratio would also result in a decrease in the passive earth pressure. In addition, the larger the soil arching effect, the greater the soil strength parameters and the interface roughness.

To facilitate the use of the proposed solutions in geotechnical engineering applications, a corrected factor of the passive earth pressure coefficient from Coulomb's theory is proposed. Furthermore, a simplified, yet accurate, design equation to evaluate such a corrected factor is also developed based on a data set involving a wide range of practical cases. Although the paper is an extension for passive earth pressure in narrow cohesive backfills, some simplified assumptions (e.g., a planar slip surface and MC failure criteria) are necessary for obtaining the solutions. In some cases, the multi- and/or curved slip surface may be formed such that using Coulomb's theory unavoidably could yield conservative results. In addition, the MC failure criteria cannot capture the nonlinear behavior of wall–soil interfaces. More future works need to be thus conducted to address these imperfections in the future. Finally, experimental works concerning the passive earth problem in narrow backfills under various movement modes can be conducted in the future.

Appendix. Variables in Eq. (70)

All the related variables that appeared in Eq. (70) are given here. It should be noted that some of the variables are simple replacements for the variables used in the derivation process of earth pressure in the upper zone. Please refer to the associated variables.

$$D'_{13} = D'_2 D'_{11} - D'_7 D'_6 \tag{76}$$

$$D'_{14} = D'_3 D'_{11} - D'_8 D'_6 \tag{77}$$

$$D'_{15} = D'_4 D'_{11} - D'_9 D'_6 \tag{78}$$

$$D'_{16} = D'_5 D'_{11} - D'_{10} D'_6 \tag{79}$$

$$D'_2 = -t'_1 D'_1 \tag{80}$$

$$D'_3 = t'_1 D'_1 + N\cos\theta'^2_w + \sin\theta'^2_w \tag{81}$$

$$D'_4 = -t'^2_1 \gamma D'^2_1 \tag{82}$$

$$D'_5 = c[\cot\phi(N\cos\theta'^2_w + \sin\theta'^2_w - 1) - D'_{12}\cos\alpha_f] \tag{83}$$

$$D'_6 = -D'_{12}(\sin\alpha_f + \tan\phi\cos\alpha_f) \tag{84}$$

$$D'_7 = -t'_2 D'_1 \tag{85}$$

$$D'_8 = t'_2 D'_1 - (N\cos\theta'^2_w + \sin\theta'^2_w)\tan\delta_1 \tag{86}$$

$$D'_9 = -\gamma\left(2t'_3 D'^2_1 - 2D'^2_1\left[\theta_s - \theta_w - \frac{\sin(\theta_s - \theta_w)}{2}\right] + \frac{1}{\tan\alpha_f}\right) \tag{87}$$

$$D'_{10} = -c[\cot\phi(N\cos\theta'^2_w + \sin\theta'^2_w)\tan\delta_1 + D'_{12}\sin\alpha_f] \tag{88}$$

$$D'_{11} = -D'_{12}(\tan\phi\sin\alpha_f - \cos\alpha_f) \tag{89}$$

$$D'_{12} = \frac{\sin\left(\frac{\theta_w + \theta_s}{2}\right)}{\sin\left(\frac{\pi}{2} + \alpha_f - \frac{\theta_w + \theta_s}{2}\right)} \tag{90}$$

$$t'_1 = \sin\theta_s - \sin\theta_w \tag{91}$$

$$t'_2 = \cos\theta_w - \cos\theta_s \tag{92}$$

$$t'_3 = \frac{\theta_s - \theta_w}{2} - \frac{\sin 2\theta_s + \sin 2\theta_w}{4} + \cos\theta_s\sin\theta_w \tag{93}$$

Data Availability Statement

All data, models, or code that support the findings of this study are available from the corresponding author upon reasonable request.

Acknowledgments

This study was supported by a CSC grant, the Postgraduate Research & Practice Innovation Program of Jiangsu Province (Grant No. KYCX20_0118), and the Scientific Research Foundation of Graduate School of Southeast University (Grant No. YBPY2041).

Notation

The following symbols are used in this paper:

B = bottom width of narrow soils behind retaining wall (m);
c = soil cohesion (kPa);
$D_1 - D_{22}$ = abbreviations used in the derivation process;
$D'_1 - D'_{22}$ = abbreviations used in the derivation process;
dz = thickness of the arched element (m);
E_p = passive earth thrust acting on rotating retaining wall (kN);
$F_x^{A_1A'_1}$, $F_x^{E_1E'_1}$ = horizontal forces at the wall–soil interface involved in the element in the upper zone (kN);
$F_x^{A_1E_1}$, $F_x^{A'_1E'_1}$ = horizontal forces on upper and lower boundaries of the element in the upper zone (kN);
$F_z^{A_1A'_1}$, $F_z^{E_1E'_1}$ = vertical forces at the wall–soil interface involved in the element in the upper zone (kN);
$F_z^{A_1E_1}$, $F_z^{A'_1E'_1}$ = vertical forces on upper and lower boundaries of the element in the upper zone (kN);
G_1 = gravity of arched differential element in the upper zone (kN);
H = retaining wall height (m);
H_1 = height of the upper zone (m);
H_2 = height of the lower zone (m);
K_p = passive thrust coefficient;
$K_{p,\text{Coulomb}}$ = passive earth pressure coefficient calculated by Coulomb's theory;
$l_{A_1E_1}$ = length of A_1E_1 (m);
$l_{E_1E'_1}$ = curve length of E_1E_1' (m);
N = ratio of major to minor principal stresses;
$p_1 - p_7$ = optimal constant coefficients;
$R_{A_1E_1}$ = radius of major principal stress trajectory (m);
z = buried depth of arched element (m);
Δz = vertical distance between points A_1 and i (m) ;
α_f = sliding angle of the slip surface (°);
β = angle of the slope (°);
γ = unit weight (kPa);
δ_1 = wall–soil interface friction angle (°);
δ_2 = slope–soil interface friction angle (°);
η = correction factor;
θ_r = rotation angle of major principal stress of the rock–soil interface in Mohr's circle (°);
θ_{r1} = rotation angle of minor principal stress on slope surface to the horizontal (°);
θ_s = rotation angle of minor principal stress on the slip surface to the horizontal (°) ;
θ_w = rotation angle of minor principal stress at the wall–soil interface to the horizontal (°);
θ'_w = rotation angle of minor principal stress at the wall–soil interface to the vertical (°);
ϕ = soil friction angle (°);
μ_1 = interface roughness factor of the wall;
μ_2 = interface roughness factor of the slope;
σ_3^0 = minor principal stresses at the wall–soil interface (kPa);
σ_3^i = minor principal stress at arbitrary point i on upper boundary of the element (kPa);
σ_w^0, σ_w^u, σ_w^l = lateral earth pressure exerted in upper and lower zones (kPa);
σ_r, τ_r = normal and shear stresses on the rock–soil surface (kPa); and
σ_s, τ_s = normal and shear stresses on the slip surface in backfills (kPa).

References

Cai, Y., Q. Chen, Y. Zhou, S. Nimbalkar, and J. Yu. 2017. "Estimation of passive earth pressure against rigid retaining wall considering arching effect in cohesive-frictional backfill under translation mode." *Int. J. Geomech.* 17 (4): 04016093. https://doi.org/10.1061/(ASCE)GM.1943-5622.0000786.

Cao, W., T. Liu, and Z. Xu. 2019a. "Calculation of passive earth pressure using the simplified principal stress trajectory method on rigid retaining walls." *Comput. Geotech.* 109: 108–116. https://doi.org/10.1016/j.compgeo.2019.01.021.

Cao, W., T. Liu, and Z. Xu. 2019b. "Estimation of active earth pressure on inclined retaining wall based on simplified principal stress trajectory method." *Int. J. Geomech.* 19 (7): 06019011. https://doi.org/10.1061/(ASCE)GM.1943-5622.0001447.

Cao, W., H. Zhang, T. Liu, and X. Tan. 2020. "Analytical solution for the active earth pressure of cohesionless soil behind an inclined retaining wall based on the curved thin-layer element method." *Comput. Geotech.* 128: 103851. https://doi.org/10.1016/j.compgeo.2020.103851.

Chen, F., Y. Lin, and D. Li. 2019. "Solution to active earth pressure of narrow cohesionless backfill against rigid retaining walls under translation mode." *Soils Found.* 59 (1): 151–161. https://doi.org/10.1016/j.sandf.2018.09.010.

Chen, F., G. Miao, and F. Lai. 2020a. "Base instability triggered by hydraulic uplift of pit-in-pit braced excavations in soft clay overlying a confined aquifer." *KSCE J. Civ. Eng.* 24 (6): 1717–1730. https://doi.org/10.1007/s12205-020-1102-2.

Chen, F.-q., C. Lin, L.-b. Lin, and M. Huang. 2021a. "Active earth pressure of narrow cohesive backfill on rigid retaining wall of rotation about the bottom." *Soils Found.* 61 (1): 95–112. https://doi.org/10.1016/j.sandf.2020.11.002.

Chen, F.-q., Y.-j. Lin, and J.-t. Yang. 2020b. "Passive earth pressure of narrow cohesionless backfill against inclined rigid retaining walls under translation mode." *Soils Found.* 60 (5): 1226–1240. https://doi.org/10.1016/j.sandf.2020.07.001.

Chen, F.-q., Y.-j. Lin, J.-t. Yang, and M. Huang. 2021b. "Passive earth pressure of narrow cohesionless backfill against rigid retaining walls rotating about the base." *Int. J. Geomech.* 21 (1): 06020036. https://doi.org/10.1061/(ASCE)GM.1943-5622.0001889.

Chen, J.-J., M.-G. Li, and J.-H. Wang. 2017. "Active earth pressure against rigid retaining walls subjected to confined cohesionless soil." *Int. J. Geomech.* 17 (6): 06016041. https://doi.org/10.1061/(ASCE)GM.1943-5622.0000855.

Fan, C.-C., and Y.-S. Fang. 2010. "Numerical solution of active earth pressures on rigid retaining walls built near rock faces." *Comput. Geotech.* 37 (7–8): 1023–1029. https://doi.org/10.1016/j.compgeo.2010.08.004.

Fang, Y.-S., T.-J. Chen, and B.-F. Wu. 1994. "Passive earth pressures with various wall movements." *J. Geotech. Eng.* 120 (8): 1307–1323. https://doi.org/10.1061/(ASCE)0733-9410(1994)120:8(1307).

Frydman, S., and I. Keissar. 1987. "Earth pressure on retaining walls near rock faces." *J. Geotech. Eng.* 113 (6): 586–599. https://doi.org/10.1061/(ASCE)0733-9410(1987)113:6(586).

Handy, R. L. 1985. "The arch in soil arching." *J. Geotech. Eng.* 111 (3): 302–318. https://doi.org/10.1061/(ASCE)0733-9410(1985)111:3(302).

Lai, F., F. Chen, and L.-L. Wan. 2018. "Vertical stresses of shallow foundations based on partially developed soil arching effect." *Rock Soil Mech.* 39 (7): 2546–2554. https://doi.org/10.16285/j.rsm.2016.2226.

Lai, F., S. Chen, J. Xue, and F. Chen. 2020a. "New analytical solutions for shallow cohesive soils overlying trench voids under various slip surfaces." *Transp. Geotech.* 25: 100411. https://doi.org/10.1016/j.trgeo.2020.100411.

Lai, F., S. Liu, Y. Deng, Y. Sun, K. Wu, and H. Liu. 2020b. "Numerical investigations of the installation process of giant deep-buried circular open caissons in undrained clay." *Comput. Geotech.* 118: 103322. https://doi.org/10.1016/j.compgeo.2019.103322.

Lai, F., S. Liu, Y. Li, and Y. Sun. 2022a. "A new installation technology of large diameter deeply-buried caissons: Practical application and observed performance." *Tunnelling Underground Space Technol.* 125: 104507. https://doi.org/10.1016/j.tust.2022.104507.

Lai, F., S. Liu, D. Yang, Y. Cheng, and Q. Fan. 2022b. "Generalized solution to active earth pressure exerted onto retaining wall with narrow backfills." *Chin. J. Geotech. Eng.* 44 (3): 1–10.

Lai, F., D. Yang, S. Liu, H. Zhang, and Y. Cheng. 2022c. "Towards an improved analytical framework to estimate active earth pressure in narrow c–ϕ soils behind rotating walls about the base." *Comput. Geotech.* 141: 104544. https://doi.org/10.1016/j.compgeo.2021.104544.

Lai, F., N. Zhang, S. Liu, Y. Sun, and Y. Li. 2021. "Ground movements induced by installation of twin large diameter deeply-buried caissons: 3D numerical modeling." *Acta Geotech.* 16 (9): 2933–2961. https://doi.org/10.1007/s11440-021-01165-1.

Li, M.-G., J.-J. Chen, and J.-H. Wang. 2017. "Arching effect on lateral pressure of confined granular material: Numerical and theoretical analysis." *Granular Matter* 19 (2): 20. https://doi.org/10.1007/s10035-017-0700-2.

Lin, Y.-j., F.-q. Chen, J.-t. Yang, and D. Li. 2020. "Active earth pressure of narrow cohesionless backfill on inclined rigid retaining walls rotating about the bottom." *Int. J. Geomech.* 20 (7): 04020102. https://doi.org/10.1061/(ASCE)GM.1943-5622.0001727.

Liu, F. Q., and J. H. Wang. 2008. "A generalized slip line solution to the active earth pressure on circular retaining walls." *Comput. Geotech.* 35 (2): 155–164. https://doi.org/10.1016/j.compgeo.2007.06.002.

Liu, F. Q., J. H. Wang, and L. L. Zhang. 2009. "Axi-symmetric active earth pressure obtained by the slip line method with a general tangential stress coefficient." *Comput. Geotech.* 36 (1–2): 352–358. https://doi.org/10.1016/j.compgeo.2008.02.002.

Maleki, M., and M. Imani. 2022. "Active lateral pressure to rigid retaining walls in the presence of an adjacent rock mass." *Arabian J. Geosci.* 15 (2): 1–11. https://doi.org/10.1007/s12517-022-09454-z.

Ni, P., L. Song, G. Mei, and Y. Zhao. 2018. "On predicting displacement-dependent earth pressure for laterally loaded piles." *Soils Found.* 58 (1): 85–96. https://doi.org/10.1016/j.sandf.2017.11.007.

O'neal, T. S., and D. J. Hagerty. 2011. "Earth pressures in confined cohesionless backfill against tall rigid walls—A case history." *Can. Geotech. J.* 48 (8): 1188–1197. https://doi.org/10.1139/t11-033.

Rui, R., Y.-q. Ye, J. Han, L. Zhang, and Y.-x. Zhai. 2020. "Experimental and theoretical investigations on active earth pressure distributions behind rigid retaining walls with narrow backfill under a translational mode." *Int. J. Geomech.* 20 (10): 04020178. https://doi.org/10.1061/(ASCE)GM.1943-5622.0001832.

Shakeel, M., and C. W. W. Ng. 2018. "Settlement and load transfer mechanism of a pile group adjacent to a deep excavation in soft clay." *Comput. Geotech.* 96: 55–72. https://doi.org/10.1016/j.compgeo.2017.10.010.

Take, W. A., and A. J. Valsangkar. 2001. "Earth pressures on unyielding retaining walls of narrow backfill width." *Can. Geotech. J.* 38 (6): 1220–1230. https://doi.org/10.1139/t01-063.

Xie, M., J. Zheng, R. Zhang, L. Cui, and C. Miao. 2020. "Active earth pressure on rigid retaining walls built near rock faces." *Int. J. Geomech.* 20 (6): 04020061. https://doi.org/10.1061/(ASCE)GM.1943-5622.0001675.

Xie, Y., and B. Leshchinsky. 2016. "Active earth pressures from a log-spiral slip surface with arching effects." *Géotechnique Lett.* 6 (2): 149–155. https://doi.org/10.1680/jgele.16.00015.

Xu, C., Q. Chen, W. Luo, and L. Liang. 2019. "Analytical solution for estimating the stress state in backfill considering patterns of stress distribution." *Int. J. Geomech.* 19 (1): 04018189. https://doi.org/10.1061/(ASCE)GM.1943-5622.0001332.

Yang, D., F. Lai, and S. Liu. 2022. "Earth pressure in narrow cohesive-fictional soils behind retaining walls rotated about the top: An analytical approach." *Comput. Geotech.* 149: 104849. https://doi.org/10.1016/j.compgeo.2022.104849.

Yang, M., and B. Deng. 2019. "Simplified method for calculating the active earth pressure on retaining walls of narrow backfill width based on DEM analysis." *Adv. Civ. Eng.* 2019: 1507825. https://doi.org/10.1155/2019/1507825.

Yang, M., and X. Tang. 2017. "Rigid retaining walls with narrow cohesionless backfills under various wall movement modes." *Int. J. Geomech.* 17 (11): 04017098. https://doi.org/10.1061/(ASCE)GM.1943-5622.0001007.

Ying, H., J. Zhang, X. Wang, B. Li, and W. Zhu. 2016. "Experimental analysis of passive earth pressure against rigid retaining wall under translation mode for finite soils." *Chin. J. Geotech. Eng.* 38 (6): 978–985. https://doi.org/10.11779/CJGE201606002.